Transitions in turbulent rotating convection: A Lagrangian perspective

Hadi Rajaei,* Pranav Joshi, Kim M. J. Alards, Rudie P. J. Kunnen, Federico Toschi, and Herman J. H. Clercx
Fluid Dynamics Laboratory, Department of Applied Physics and J. M. Burgers Center for Fluid Dynamics, Eindhoven University of Technology, P.O. Box 513, 5600 MB Eindhoven, the Netherlands
(Received 17 November 2015; published 29 April 2016)

Using measurements of Lagrangian acceleration in turbulent rotating convection and accompanying direct numerical simulations, we show that the transition between turbulent states reported earlier [e.g., S. Weiss *et al.*, Phys. Rev. Lett. **105**, 224501 (2010)] is a boundary-layer transition between the Prandtl-Blasius type (typical of nonrotating convection) and Ekman type.

DOI: 10.1103/PhysRevE.93.043129

I. INTRODUCTION

Turbulent flow in a rotating environment is common in nature and technology. Prime examples are geophysical and astrophysical flows, including oceanic and atmospheric currents [1–4] and the convective outer layer of the Sun [5], as well as convective cooling in turbomachinery [6,7] and chemical vapor deposition on rotating substrates [8].

A simple laboratory realization of these flows, allowing fundamental investigation, is rotating Rayleigh-Bénard convection (RRBC), the flow between two rotating horizontal plates heated from below and cooled from above. The influence of the Coriolis force lets the flow depart significantly from the nonrotating situation. In particular, a sudden transition between two different turbulent states has been described in this system [9–12]. Sudden transitions are unexpected in vigorous turbulence. The transition is usually detected as an abrupt change in the heat transfer scaling, but the effect on the flow organization is more dramatic, changing from the domain-filling large-scale circulation (LSC) [13] at lower rotation rates to an ensemble of rotation-aligned vortical plumes emerging from top and bottom boundary layers with positive (cyclonic) vorticity fed by so-called Ekman pumping [14,15]. The transition was explained to be due to finiteness of the domain [11], thus the result is setup specific.

In this study we use Lagrangian acceleration statistics from three-dimensional (3D) particle-tracking velocimetry (3D-PTV) and direct numerical simulations (DNSs) to show that the transition is actually a boundary-layer (BL) transition independent of the flow geometry: while the bulk flow is largely unaffected, the kinetic BLs on the plates transition between the Prandtl-Blasius [13] and Ekman type [15,16]. This sudden BL transition will thus take place independently of geometry and is a generic feature of rotating buoyancy-driven turbulence near walls. Additionally, we find that the bulk flow gradually changes as rotation is increased beyond the transition, so that another regime change is due once the entire bulk becomes rotationally constrained [17]; i.e., it adheres primarily to the so-called geostrophic balance between Coriolis forces and pressure gradient [15,16]. In this constrained regime the convective heat transfer is reduced and can even be suppressed altogether [18].

The Lagrangian exploration of Rayleigh-Bénard convection (RBC) has been done numerically [19,20] and experimentally [21,22], but not under rotation. Here we extend this method to the rotating frame.

The remainder of the paper is organized as follows. The experimental and numerical setups are discussed in Sec. II. In Sec. III the experimental and numerical results on the particle acceleration and viscous boundary layers are presented and discussed. We summarize our main findings in Sec. IV.

II. METHODS AND PARAMETERS

The experiment consists of a cylindrical Plexiglas vessel and a 3D-PTV system. The vessel, of equal height and diameter $L = D = 200$ mm, is closed with a copper plate at the bottom and a transparent cooling chamber at the top. For technical details, see Ref. [23].

The working fluid, water, is seeded with polyethylene particles (density $\rho = 1002\,\mathrm{kg/m^3}$, diameter $d_p = 75$–$90\,\mu$m), which are illuminated by four LED arrays. Images are recorded by four CCD cameras (MegaPlus ES2020, 1600×1200 pixels) located above the convection cell. Images are recorded at 30 Hz, which is sufficient to capture the smallest scales of motion with Kolmogorov time scales on the order of seconds. Two sets of measurements are performed: (i) in the cell center and (ii) near the top plate. The measurement volume is $50 \times 50 \times 50\ \mathrm{mm^3}$ (x,y,z) at the center and $50 \times 50 \times 10\ \mathrm{mm^3}$ (x,y,z) near the top plate with its center on the cylinder axis. The measurement volume near the top is up to the plate surface. The z axis coincides with the rotation axis and gravity. Based on the DNSs we know that the viscous boundary layer near the top has a thickness between 1.6 and 6 mm, depending on the rotation rate.

The images are processed using a PTV code developed at ETH Zürich [24–28]. The seeding density is limited to ~1500 particles per image. To eliminate background noise in the measurements, cubic polynomial fitting described in Ref. [29] is implemented. The four nondimensional parameters that describe RRBC are the Rayleigh number $\mathrm{Ra} = \alpha g \Delta T L^3/(\kappa\nu)$, Prandtl number $\mathrm{Pr} = \nu/\kappa$, convective Rossby number $\mathrm{Ro} = \sqrt{\alpha g \Delta T/L}/(2\Omega)$ (ratio of buoyancy and Coriolis forces), and aspect ratio $\Gamma = D/L$, where g is the gravitational acceleration, ΔT the applied temperature difference, Ω the rotation rate, and α,ν, and κ are the thermal expansion coefficient, kinematic viscosity, and thermal diffusivity of the fluid, respectively. In the present work $\mathrm{Ra} = 1.28 \times 10^9, \mathrm{Pr} =$

*h.rajaei@tue.nl

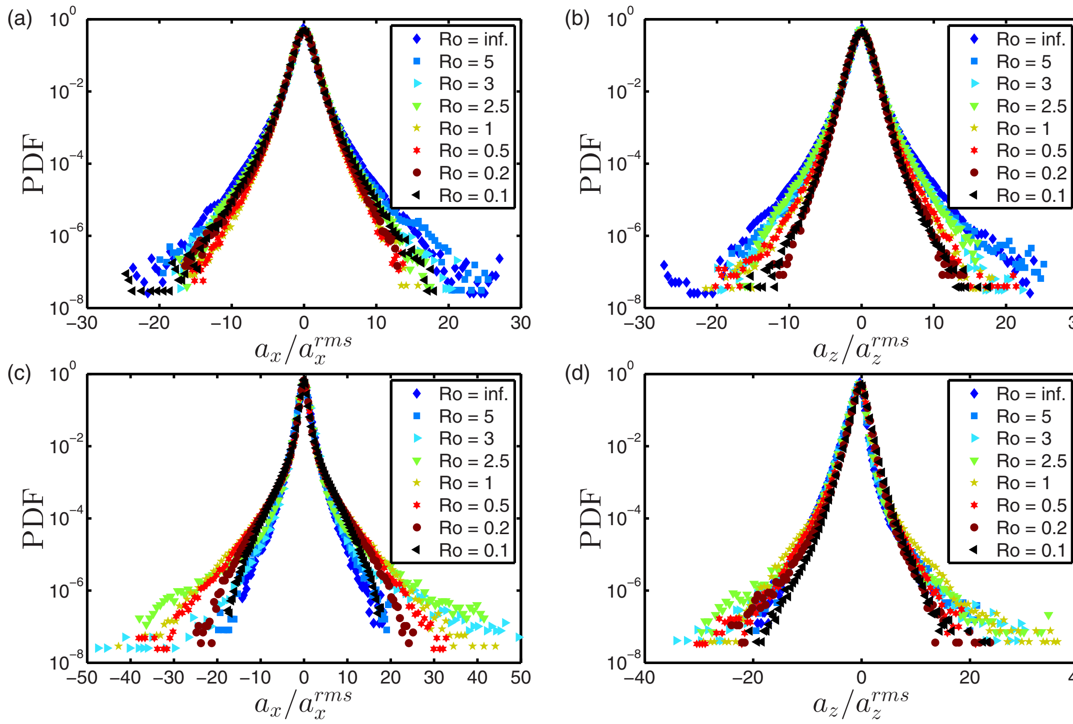

FIG. 1. Normalized acceleration PDFs from experiments for Ra $= 1.28 \times 10^9$, Pr $= 6.7$, and $\Gamma = 1$: (a) horizontal at the center, (b) vertical at the center, (c) horizontal near top (larger horizontal axis range compared to other PDFs), and (d) vertical near top.

6.7, and $\Gamma = 1$ are kept fixed while Ro is varied between 0.1 and ∞ (Ω between 1.65 rad/s and 0). Each experiment lasts roughly 300 min (consisting of multiple segments, each 11 min long). The number of data points for each experiment is $\sim 7 \times 10^7$ at the center and $\sim 3.5 \times 10^7$ near the top plate. DNSs have been performed in parallel to the experiments. Here we briefly mention the numerical approach; details can be found in Ref. [30]. The governing Boussinesq equations are discretized with a second-order central finite-difference scheme in cylindrical coordinates. We track the motion of pointlike passive tracer particles with flow velocity obtained from trilinear interpolation. Time integration for the flow uses a third-order Runge-Kutta scheme; for the tracers a second-order Adams-Bashforth scheme is applied. The spatial grid resolution in radial, azimuthal and vertical directions is $384 \times 512 \times 512$, respectively, with grid refinement close to the plates and sidewall.

III. RESULTS AND DISCUSSION

To show the effects of rotation on the convective flow, we consider probability distribution functions (PDFs) of acceleration in the center and close to the top plate, separated into horizontal and vertical components.

Figure 1(a) shows the normalized experimental horizontal-acceleration PDFs in the cell center. The shapes of the horizontal-acceleration PDFs are largely independent of Ω; they nearly collapse (except for the tails). This is further exemplified by the kurtosis values $K_i = \langle a_i^4 \rangle / \langle a_i^2 \rangle^2$, plotted in Fig. 2(a) (cyan triangles). All representative variables for the horizontal directions are obtained by averaging the respective variables along x and y directions. The transition point at $\mathrm{Ro}_c \cong 2.5$ [11] is indicated by the vertical dash-dotted line. A weak nonmonotonic trend for the width of the horizontal-acceleration PDFs at the center is noticeable

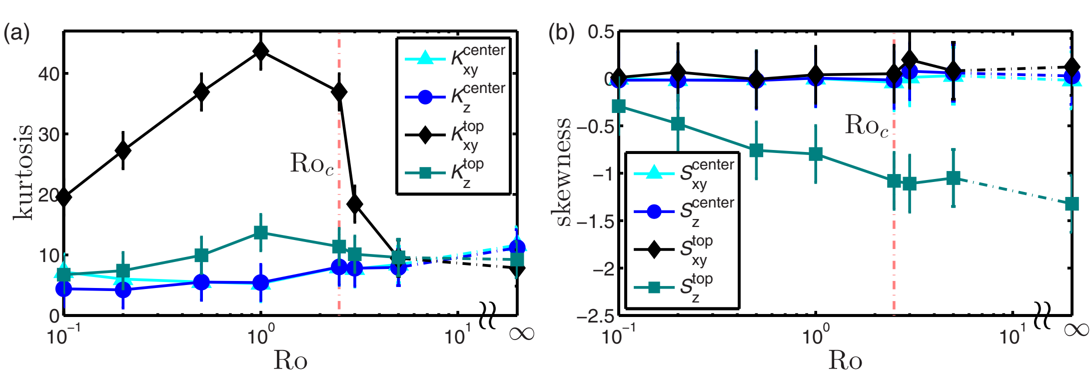

FIG. 2. (a) Kurtosis and (b) skewness of experimental acceleration PDFs as a function of Ro.

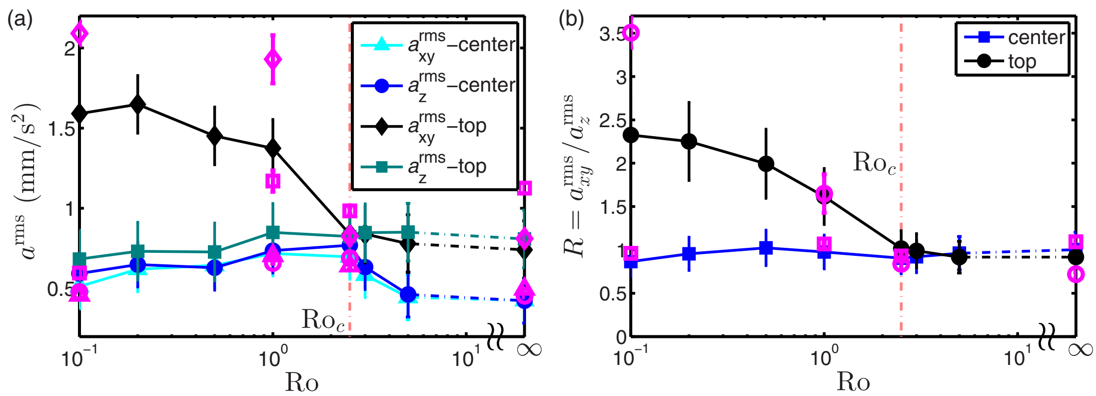

FIG. 3. (a) Acceleration rms values and (b) the ratio $R = a_{xy}^{\rm rms}/a_z^{\rm rms}$ as a function of Ro. Purple open symbols represent DNS data for corresponding experiments (marker shapes match). Experimental acceleration uncertainty is estimated by adding noise to the displacement, with an rms value equal to that of displacement measured for points on a fixed target inside the RB cell. The uncertainty in DNSs is estimated as the deviation from the expected flow symmetry.

as a function of Ro: it has a local minimum at Ro ≈ 0.5. The wider PDF tails at higher and lower Ro indicate a more intermittent distribution, which is due to the presence of coherent structures. At low enough Ro the vertical plumes can actually enter into the center, a sign of adaptation to rotation of the bulk flow. However, note that $K_{xy}^{\rm center}$ does not show significant changes around Ro$_c$. The horizontal-acceleration PDFs in the center are symmetrical, evidenced by the skewness $S_i = \langle a_i^3\rangle/\langle a_i^2\rangle^{3/2}$ being basically zero for all Ro [Fig. 2(b)]. Finally, we present the rms values of horizontal acceleration, $a_{xy}^{\rm rms} = (a_x^{\rm rms} + a_y^{\rm rms})/2$, in the center in Fig. 3(a). The Lagrangian rms acceleration shows a broad maximum between $1 \lesssim$ Ro $\lesssim 2.5$, while at lower Ro it is suppressed by rotation.

The vertical-acceleration PDFs in the center are depicted in Fig. 1(b). The PDFs are progressively narrower for lower Ro, as is also clear from the kurtosis [Fig. 2(a), blue circles]. The PDFs are symmetric [Fig. 2(b)]. The rms value of vertical acceleration in the center displays a similar behavior as its horizontal counterpart [Fig. 3(a)]. The suppression of high-acceleration events along the rotation axis with increasing rotation has been observed before in experiments on rotating turbulence [31].

The ratio $R = a_{xy}^{\rm rms}/a_z^{\rm rms}$ in the center [see Fig. 3(b), blue squares] is largely independent of Ro and unaffected by the transition at Ro$_c$. Only at the lowest Ro a slight downward trend can be observed. However, the downward trend is rather insignificant. We conclude that the shapes of the acceleration PDFs as well as the isotropy of acceleration in the cell center are largely unaffected while crossing Ro$_c$.

Continuing with the measurements near the top plate, the results change drastically. The horizontal-acceleration PDFs in Fig. 1(c) (note that the horizontal axis range is larger compared to other PDFs) reveal a strong dependence on Ro with very wide tails at Ro ≈ 1 and narrower distributions for both higher and lower Ro. This trend is emphasized in the kurtosis plot in Fig. 2(a) (black diamonds), where a huge jump occurs at Ro$_c$. Just below Ro$_c$ there is a significantly enhanced probability of extreme acceleration events. This is evidence of the BL transitioning from (nonrotating) Prandtl-Blasius to (rotating) Ekman type. Due to Ekman pumping the converging flow feeding a plume spins up cyclonically [32]. This swirling flow greatly enhances horizontal acceleration as also found in the acceleration rms values in Fig. 3(a). The PDFs remain symmetric at all Ro [Fig. 2(b)] given that within the vortical structures both horizontal directions are equivalent.

The PDFs of vertical acceleration near the top plate in Fig. 1(d) are negatively skewed [see also Fig. 2(b), turquoise squares]: negative vertical-acceleration events are confined to small areas but with large magnitudes, a sign of formation of coherent structures near the plates at all Ro. However, as Ro decreases the skewness is reduced. Similar strong localized events have been observed for Eulerian velocity as well [32]. $K_z^{\rm top}$ steps up (milder compared to $K_{xy}^{\rm top}$) at Ro$_c$ [Fig. 2(a)], while getting progressively smaller for lower Ro. $a_z^{\rm rms}$ near the top is unaffected by rotation for Ro $>$ Ro$_c$, while showing a similar decrease as the central rms values below Ro$_c$. Both horizontal and vertical acceleration rms values in the cell center, plotted in Fig. 3(a), increase when Ro approaches Ro$_c$ from the nonrotating side, while rms values at the top show no changes.

The ratio R near the top plate, as depicted in Fig. 3(b) (black circles), reveals again the BL transition at Ro$_c$: due to Ekman pumping the acceleration becomes strongly anisotropic below Ro$_c$, while being isotropic above. This is in stark contrast with the center, which remains isotropic. Anisotropy of acceleration displays a trend different from that of Eulerian velocity. Eulerian velocity statistics show an enhancement in anisotropy at the center and a decrease near the top with increase in Ω [33].

Purple open symbols (with the same shapes) represent DNS data for corresponding experiments in Figs. 3(a)–(b). Apart from the lower magnitudes of the experimental data, the trends for DNS and experiments are similar. The results of DNSs and experiments deviate for the horizontal component near the top due to a reduced likelihood of capturing high-acceleration events in the experiment. DNSs and experiments match at the center since the acceleration rms are generally lower. The DNS data for skewness and kurtosis show similar trends as the experiments; however, the values are generally higher (by ∼20%–100%). Since kurtosis and skewness are highly sensitive to extreme events the error bars are large. Therefore, we are more interested in the trends rather than the actual values.

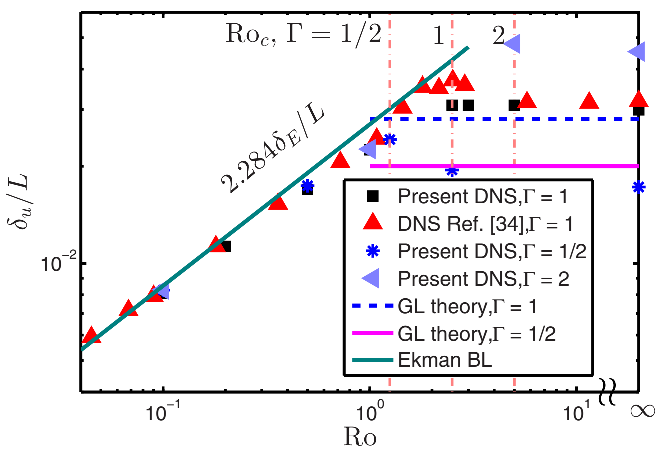

FIG. 4. Normalized BL thickness as a function of Ro. The three vertical lines represent transitions for $\Gamma = 1/2$, 1 and 2.

For further confirmation of the BL transition, we consider the DNS data for three aspect ratios: 1/2, 1, and 2. Following Refs. [10,34,35], we define the thickness of the kinematic BL, δ_u, as the position of the maximum horizontal rms velocity. Figure 4 shows the δ_u for the present DNS data and that of Ref. [34] (at $\mathrm{Ra} = 1 \times 10^9, \mathrm{Pr} = 6.4$). In addition to DNSs, we estimate δ_u for the nonrotating case employing Grossmann-Lohse (GL) theory [36–40] for $\Gamma = 1$ and 1/2: $\delta_u = aL/\sqrt{\mathrm{Re}}$ [36,38] where $a \approx 0.922$ (0.684) for $\Gamma = 1$ (1/2) [40]. The blue dashed and magenta solid lines in Fig. 4 show the theoretical (Prandtl-Blasius) BL thickness based on GL theory for $\Gamma = 1$ and 1/2, respectively. They match well with the DNS data for corresponding Γ. Close to the transition at Ro_c these theoretical estimates no longer hold, as rotation starts to change the BL dynamics.

We use linear Ekman BL theory to describe the BLs under rotation. The problem of the matching of a geostrophic bulk flow with velocity U in x direction to a solid boundary can be easily solved [16]:

$$u = U[1 - e^{-z/\delta_E}\cos(z/\delta_E)], \qquad (1a)$$

$$v = Ue^{-z/\delta_E}\sin(z/\delta_E)\,, \qquad (1b)$$

where u and v are the horizontal velocity components in the Ekman BL, $\delta_E = \sqrt{\nu/\Omega}$ is the characteristic Ekman BL thickness, and z is the distance to the plate. Note that δ_E is independent of the exterior velocity and the flow geometry. This generic solution suffices for RRBC simulations where the orientation of the LSC is not fixed to the coordinate system. The BL velocity actually possesses a maximum $\sqrt{u^2 + v^2} = 1.069U$ at $z/\delta_E = 2.284$, before asymptotically reducing to U at larger z. This theoretical prediction based on linear BL theory accurately describes the turbulent simulation data including the prefactor; see the turquoise line in Fig. 4. We conclude that indeed the BLs change from Prandtl-Blasius to Ekman type at Ro_c. The applicability of Ekman theory has been validated in a wide parameter range [34,41–44]. There is no primary dependence on Ra or Pr.

IV. CONCLUSION

Using Lagrangian acceleration statistics and accompanying DNS, we find an abrupt transition in the BL dynamics of RRBC between Prandtl-Blasius type and Ekman type BLs. This transition in BLs coincides with the transition reported earlier and predicted surprisingly well by employing Ginzburg-Landau theory in Ref. [11]. Our analysis contributes to the understanding of the transition by describing the physics of the BLs which drive this process. The BLs related to the LSC are of Prandtl-Blasius type; as their characteristic thickness δ_u becomes comparable to δ_E the transition occurs and the vortical plumes aid in the disappearance of the LSC [9].

We have presented the first measurement of Lagrangian acceleration in rotating Rayleigh-Bénard convection. 3D-PTV and DNSs have revealed that the turbulent transition in RRBC is a boundary-layer transition. Posttransition, where the BL is already rotation-dominated, the bulk becomes progressively affected by rotation: fluctuations are reduced and vortical plumes can enter deeper into the bulk, leading to opposite trends in the kurtosis of vertical and horizontal accelerations. We expect that the subsequent regime change at high rotation happens when the entire bulk becomes rotation-dominated [17].

ACKNOWLEDGMENTS

This work is supported by the Foundation for Stichting voor Fundamenteel Onderzoek der Materie (FOM), the Netherlands. The authors gratefully acknowledge the support of the Nederlandse Organisatie voor Wetenschappelijk Onderzoek (NWO) for the use of supercomputer facilities (Cartesius) under Grants No. SH-202 and SH-334.

[1] J. Marshall and F. Schott, Rev. Geophys. **37**, 1 (1999).
[2] J. Gascard, A. J. Watson, M. J. Messias, K. A. Olsson, T. Johannessen, and K. Simonsen, Nature (London) **416**, 525 (2002).
[3] P. Wadhams, J. Holfort, E. Hansen, and J. P. Wilkinson, Geophys. Res. Lett. **29**, 1434 (2002).
[4] D. L. Hartmann, L. A. Moy, and Q. Fu, J. Climate **14**, 4495 (2001).
[5] M. S. Miesch, Solar Phys. **192**, 59 (2000).
[6] M. G. Dunn, J. Turbomach. **123**, 637 (2001).
[7] J. P. Johnston, Int. J. Rot. Mach. **4**, 97 (1998).
[8] H. Van Santen, C. R. Kleijn, and H. E. A. Van Den Akker, J. Cryst. Growth **212**, 299 (2000).
[9] R. P. J. Kunnen, H. J. H. Clercx, and B. J. Geurts, Europhys. Lett. **84**, 24001 (2008).
[10] R. J. A. M. Stevens, J.-Q. Zhong, H. J. H. Clercx, G. Ahlers, and D. Lohse, Phys. Rev. Lett. **103**, 024503 (2009).
[11] S. Weiss, R. J. A. M. Stevens, J.-Q. Zhong, H. J. H. Clercx, D. Lohse, and G. Ahlers, Phys. Rev. Lett. **105**, 224501 (2010).
[12] P. Wei, S. Weiss, and G. Ahlers, Phys. Rev. Lett. **114**, 114506 (2015).

[13] G. Ahlers, S. Grossmann, and D. Lohse, Rev. Mod. Phys. **81**, 503 (2009).
[14] R. J. A. M. Stevens, H. J. H. Clercx, and D. Lohse, Eur. J. Mech. B **40**, 41 (2013).
[15] J. Pedlosky, *Geophysical Fluid Dynamics*, 2nd ed. (Springer, Berlin, 1987).
[16] P. K. Kundu and I. M. Cohen, *Fluid Mechanics*, 2nd ed. (Academic Press, London, 2002).
[17] K. Julien, E. Knobloch, A. M. Rubio, and G. M. Vasil, Phys. Rev. Lett. **109**, 254503 (2012).
[18] S. Chandrasekhar, *Hydrodynamic and Hydromagnetic Stability* (Oxford University Press, Oxford, 1961).
[19] J. Schumacher, Phys. Rev. E **79**, 056301 (2009).
[20] M. S. Emran and J. Schumacher, Phys. Rev. E **82**, 016303 (2010).
[21] R. Ni, S.-D. Huang, and K.-Q. Xia, Phys. Rev. Lett. **107**, 174503 (2011).
[22] R. Ni, S.-D. Huang, and K.-Q. Xia, J. Fluid Mech. **692**, 395 (2012).
[23] R. P. J. Kunnen, Y. Corre, and H. J. H. Clercx, Europhys. Lett. **104**, 54002 (2013).
[24] H. G. Maas, A. Gruen, and D. Papantoniou, Exp. Fluids **15**, 133 (1993).
[25] N. A. Malik, T. Dracos, and D. A. Papantoniou, Exp. Fluids **15**, 279 (1993).
[26] J. Willneff, Ph.D. thesis, Swiss Federal Institute of Technology, Zürich, Switzerland, 2003.
[27] J. Willneff, Int. Arch. Photogramm. Rem. Sens. Spatial Inform. Sci. **34**, 601 (2002).
[28] B. Lüthi, A. Tsinober, and W. Kinzelbach, J. Fluid Mech. **528**, 87 (2005).
[29] B. Lüthi, Ph.D. thesis, Swiss Federal Institute of Technology, Zürich, Switzerland, 2002.
[30] R. Verzicco and R. Camussi, J. Fluid Mech. **477**, 19 (2003).
[31] L. Del Castello and H. J. H. Clercx, Phys. Rev. Lett. **107**, 214502 (2011).
[32] R. P. J. Kunnen, H. J. H. Clercx, and B. J. Geurts, Phys. Rev. E **74**, 056306 (2006).
[33] R. P. J. Kunnen, H. J. H. Clercx, and B. J. Geurts, Phys. Rev. Lett. **101**, 174501 (2008).
[34] R. P. J. Kunnen, B. J. Geurts, and H. J. H. Clercx, J. Fluid Mech. **642**, 445 (2010).
[35] E. M. King, S. Stellmach, J. Noir, U. Hansen, and J. M. Aurnou, Nature (London) **457**, 301 (2009).
[36] S. Grossmann and D. Lohse, J. Fluid Mech. **407**, 27 (2000).
[37] S. Grossmann and D. Lohse, Phys. Rev. Lett. **86**, 3316 (2001).
[38] S. Grossmann and D. Lohse, Phys. Rev. E **66**, 016305 (2002).
[39] S. Grossmann and D. Lohse, Phys. Fluids **16**, 4462 (2004).
[40] R. J. A. M. Stevens, E. P. van der Poel, S. Grossmann, and D. Lohse, J. Fluid Mech. **730**, 295 (2013).
[41] R. P. J. Kunnen, R. J. A. M. Stevens, J. Overkamp, C. Sun, G. J. F. van Heijst, and H. J. H. Clercx, J. Fluid Mech. **688**, 422 (2011).
[42] R. P. J. Kunnen, H. J. H. Clercx, and G. J. F. van Heijst, J. Fluid Mech. **727**, 509 (2013).
[43] R. P. J. Kunnen, R. Ostilla-Mónico, E. P. van der Poel, R. Verzicco, and D. Lohse, arXiv:1409.6469v2.
[44] S. Stellmach, M. Lischper, K. Julien, G. Vasil, J. S. Cheng, A. Ribeiro, E. M. King, and J. M. Aurnou, Phys. Rev. Lett. **113**, 254501 (2014).